

Search for New Physics Involving Top Quarks at ATLAS

T. Golling on behalf of ATLAS

Department of Physics, Yale University, New Haven, CT, USA

Two searches for new phenomena involving top quarks are presented: a search for a top partner in $t\bar{t}$ events with large missing transverse momentum, and a search for $t\bar{t}$ resonances in proton-proton collisions at a center-of-mass energy of 7 TeV. The measurements are based on 35 pb⁻¹ and 200 pb⁻¹ of data collected with the ATLAS detector at the LHC in 2010 and 2011, respectively. No evidence for a signal is observed. The first limits from the LHC are established on the mass of a top partner, excluding a mass of 275 GeV for a neutral particle mass less than 50 GeV and a mass of 300 GeV for a neutral particle mass less than 10 GeV. Using the reconstructed $t\bar{t}$ mass spectrum, limits are set on the production cross-section times branching ratio to $t\bar{t}$ for narrow and wide resonances. For narrow Z' models, the observed 95% C.L. limits range from approximately 38 pb to 3.2 pb for masses going from $m_{Z'} = 500$ GeV to $m_{Z'} = 1300$ GeV. In Randall-Sundrum models, Kaluza-Klein gluons with masses below 650 GeV are excluded at 95% C.L.

1. Introduction

The Standard Model of particle physics is believed to be an effective theory valid up to energies close to 1 TeV. However, no new physics beyond the Standard Model (SM) has been observed yet, and it is critical to explore a wide range of possible signatures. A promising avenue lies in final states that involve the heaviest of the particles presumed to be elementary: the top quark. This document describes two searches for new phenomena involving top quarks using the ATLAS detector [1] at the CERN Large Hadron Collider (LHC).

The first search is carried out for a pair-produced exotic top partner (T), decaying to a top-antitop pair and two stable, neutral weakly-interacting particles (A_0 , which in some models may be its own anti-particle) [2]. In most models, the T has typical quark-like quantum numbers, and is produced through $q\bar{q}$ annihilation and gluon fusion. The final state for such a process ($T\bar{T} \rightarrow t\bar{t}A_0A_0$) is identical to $t\bar{t}$, though with a larger amount of missing transverse momentum (E_T^{miss}) from the undetected A_0 's. In supersymmetry models with R -parity conservation T refers to the stop squark and A_0 refers to the lightest supersymmetric particle. The $t\bar{t} + E_T^{\text{miss}}$ [3] signature appears in a general set of dark matter-motivated models, as well as in other SM extensions, such as the mentioned supersymmetry models, little Higgs models with T -parity conservation [4, 5], models of universal extra dimensions (UED) with Kaluza-Klein-parity [6], models in which baryon and lepton number conservation arises from gauge symmetries [7] or models with third generation scalar leptoquarks [8]. Many of these models provide a mechanism for electroweak symmetry breaking and predict dark matter candidates, which can be identified indirectly through their large E_T^{miss} signature. The search is carried out in the $t\bar{t}$ lepton+jets channel where one W boson from the top quark decay decays leptonically (including τ decays to e or μ) and the other W boson decays hadronically, resulting in a final state with an isolated lepton of high transverse momentum, four or more jets and large E_T^{miss} .

A second search is carried out for new heavy particles decaying to $t\bar{t}$ pairs [9]. Using the lepton+jets channel the reconstructed $t\bar{t}$ mass spectrum, based on three or four jets, an electron or muon, and a neutrino, is used to search for a signal. Previous searches for $t\bar{t}$ were most recently carried out by the CDF [10, 11] and D0 [12] collaborations at Run II of the Fermilab Tevatron Collider, and the ATLAS [13] and CMS [14] collaborations at the CERN LHC. No evidence for new particles was uncovered and 95% confidence level (C.L.) limits were set on the mass of a leptophobic topcolour Z' boson [15] at $m_{Z'} > 725$ [10] GeV¹ as well as on the coupling strength of a heavy colour-octet vector particle. This analysis is very similar to the previous ATLAS analysis [13] but uses data collected in 2011. The benchmark model used to quantify the experimental sensitivity to narrow resonances is a topcolour Z' boson [16] arising in models of strong electroweak symmetry breaking through top quark condensation [17]. The specific model used is the leptophobic scenario, model **IV** in Ref. [16] with $f_1 = 1$ and $f_2 = 0$ and a width of 1.2% of the Z'_t boson mass. This is the same set of parameters that was used by the D0 Collaboration [12]. The model used for wide resonances is a Kaluza-Klein gluon g_{KK} , which appears in Randall-Sundrum (RS) models with a warped extra dimension in which particles are located in the extra dimension [18, 19]. The concrete model used is described in detail in Ref. [20] and implemented in the MADGRAPH [21] event generator. The couplings to quarks take the “standard” RS values [18]: $g_L = g_R = -0.2$

¹Preliminary results from CDF and D0 exclude a mass below 900 and 820 GeV respectively.

for light quarks including charm, $g_L = 1.0, g_R = -0.2$ for bottom quarks and $g_L = 1.0, g_R = 4.0$ for the top quark. In this case, the resonance is predicted to be significantly wider than the detector and reconstruction algorithm's resolution. This model is taken as a proxy for coloured resonances.

2. The ATLAS Detector

The ATLAS detector [1] consists of an inner detector tracking system (ID) surrounded by a superconducting solenoid providing a 2 T magnetic field, electromagnetic and hadronic calorimeters, and a muon spectrometer (MS). The ID consists of pixel and silicon microstrip detectors inside a transition radiation tracker (TRT) which provide tracking in the region $|\eta| < 2.5$. The electromagnetic calorimeter is a lead/liquid-argon (LAr) detector in the barrel ($|\eta| < 1.475$)² and the endcap ($1.375 < |\eta| < 3.2$) regions. Hadron calorimetry is based on two different detector technologies. The barrel ($|\eta| < 0.8$) and extended barrel ($0.8 < |\eta| < 1.7$) calorimeters are composed of scintillator/steel, while the hadronic endcap calorimeters ($1.5 < |\eta| < 3.2$) are LAr/copper. The forward calorimeters ($3.1 < |\eta| < 4.9$) are instrumented with LAr/copper and LAr/tungsten, providing electromagnetic and hadronic energy measurements, respectively. The MS consists of three large superconducting toroids with 24 coils, a system of trigger chambers, and precision tracking chambers which provide muon momentum measurements out to $|\eta|$ of 2.7.

3. Data Samples

The search for a pair-produced exotic top partner is based on data recorded by the ATLAS detector in 2010 using 35 pb^{-1} of integrated luminosity. The search for $t\bar{t}$ resonances is based on data recorded in 2011 using 200 pb^{-1} . The data were collected using electron and muon triggers. Requirements of good beam conditions, detector performance and data quality are imposed.

4. Simulated Samples

Monte Carlo (MC) event samples with full ATLAS detector simulation [22] based on the GEANT4 program [23] and corrected for all known detector effects are used to model the signal process and most of the backgrounds. The QCD multi-jet background is modeled using data control samples rather than the simulation. The $t\bar{t}$ and single top samples are produced with MC@NLO [24], while the W +jets and Z +jets samples are generated with ALPGEN [25]. HERWIG [26] is used to simulate the parton shower and fragmentation, and JIMMY [27] is used for the underlying event simulation. The diboson background is simulated using HERWIG. The inclusive W +jets and Z +jets cross sections are normalized to NNLO predictions [28], and the cross sections of the other backgrounds are normalized to NLO predictions [29].

MADGRAPH [21] is used to simulate the signal process, and PYTHIA [30] is used to simulate the parton shower and fragmentation. A grid of T and A_0 masses is generated with $250 \text{ GeV} \leq m(T) \leq 350 \text{ GeV}$ and $10 \text{ GeV} \leq m(A_0) \leq 100 \text{ GeV}$. In this search, only on-shell tops are considered, and therefore grid points where the mass difference between the T and A_0 approaches the top quark mass are excluded. Each sample is normalized to the cross section calculated at approximate NNLO in QCD using HATHOR [31], ranging from 20.5 pb for a T mass of 250 GeV to 3.0 pb for a T mass of 350 GeV .

Signal samples for Z' bosons decaying to $t\bar{t}$ are generated using PYTHIA allowing all top quark decay modes. Samples of RS gluons are generated with MADGRAPH, and showered with PYTHIA.

5. Common Event Selection

Electron and muon candidates are selected as for other recent top quark studies using the lepton+jets signature [32]. Jets are reconstructed using the anti- k_t [33] algorithm with a distance parameter R , defined as

²The azimuthal angle ϕ is measured around the beam axis and the polar angle θ is the angle from the beam axis. The pseudorapidity is defined as $\eta \equiv -\ln \tan(\theta/2)$.

$\Delta R \equiv \sqrt{\Delta\eta^2 + \Delta\phi^2}$, of 0.4. To take into account the differences in calorimeter response to electrons and hadrons, a p_T - and η -dependent factor, derived from simulated events and validated with data, is applied to each jet to provide an average energy scale correction [34] back to particle level. In the calorimeter, the energy deposited by particles is reconstructed in three-dimensional clusters. The energy of these clusters is summed vectorially, and the projection of this sum in the transverse plane corresponds to the negative of the E_T^{miss} [35]. Corrections to the hadronic and electromagnetic energy scales, dead material and out-of-cluster energy are applied, and in the case of reconstructed muons, an additional correction is included.

Events are selected with exactly one electron or muon, where each lepton is required to pass the following selection criteria. Electrons are required to satisfy $E_T > 20$ GeV ($E_T > 25$ GeV for the resonance search due to tighter trigger requirements in 2011) and $|\eta| < 2.47$. Electrons in the transition region between the barrel and the endcap electromagnetic calorimeters ($1.37 < |\eta| < 1.52$) are removed. Muon candidates are required to satisfy $p_T > 20$ GeV and $|\eta| < 2.5$. Events with four or more reconstructed jets with $p_T > 20$ GeV ($p_T > 25$ GeV for the resonance search) and $|\eta| < 2.5$ are selected.

5.1. Additional Selection for Top Partner Search

To reduce the W +jets background, events are required to have $E_T^{\text{miss}} > 80$ GeV and $m_T > 120$ GeV, where m_T is the transverse mass of the lepton and missing energy³. Events with either a second lepton candidate satisfying looser selection criteria or an isolated track with $p_T > 12$ GeV are rejected in order to reduce the contribution from $t\bar{t}$ dilepton events. In particular the isolated track veto is useful for eliminating single-prong hadronic τ decays in $t\bar{t}$ dilepton events.

5.2. Additional Selection for Resonance Search

In the electron channel, E_T^{miss} must be larger than 35 GeV and $m_T(\text{lepton}, E_T^{\text{miss}}) > 25$ GeV. In the muon channel, $E_T^{\text{miss}} > 20$ GeV and $E_T^{\text{miss}} + m_T(\text{lepton}, E_T^{\text{miss}}) > 60$ GeV is required. At least one of the selected jets must be tagged as a b -jet.

Jets originating from b -quarks are selected by exploiting the long lifetimes of B -hadrons (about 1.5 ps) leading to typical flight paths of a few millimeters, which are observable in the detector. The SV0 b -tagging algorithm [36] used in this analysis explicitly reconstructs a displaced vertex from the decay products of the long-lived B -hadron. Two-track vertices at a radius consistent with the radius of one of the three pixel detector layers are removed, as these vertices likely originate from material interactions. A jet is considered b -tagged if it contains a secondary vertex, reconstructed with the SV0 tagging algorithm, with $L/\sigma(L) > 5.85$, where L is the decay length and $\sigma(L)$ its uncertainty. This operating point yields a 50% b -tagging efficiency in simulated $t\bar{t}$ events. The sign of $L/\sigma(L)$ is given by the sign of the projection of the decay length vector on the jet axis.

6. Background Estimate for Top Partner Search

A summary of the background estimates and a comparison with the observed number of selected events passing all selection criteria is shown in Table I. A total yield of 17.2 ± 2.6 events is expected from SM sources, and 17 events are observed in data. The background composition is similar in the electron and muon channels.

Table I: Summary of expected SM yields including statistical and systematic uncertainties compared with the observed number of events in the signal region.

Source	single lepton $t\bar{t}/W$ +jets	dilepton $t\bar{t}$	multi-jet	Z +jets	dibosons	single top	total	data
Number of events	8.4 ± 1.6	7.6 ± 2.0	0.2 ± 0.6	0.4 ± 0.1	$0.2 \pm <0.1$	0.4 ± 0.1	17.2 ± 2.6	17

³The transverse mass is defined by the formula $m_T = \sqrt{2p_T^\ell E_T^{\text{miss}}(1 - \cos(\phi^\ell - \phi^{E_T^{\text{miss}}}))}$, where p_T^ℓ is the p_T (E_T) of the muon (electron) and ϕ^ℓ ($\phi^{E_T^{\text{miss}}}$) is the azimuthal angle of the lepton (E_T^{miss}).

The dominant background arises from $t\bar{t}$ dilepton final states, in which one of the leptons is not reconstructed, is outside the detector acceptance, or is a τ lepton. In all such cases, the $t\bar{t}$ decay products include two high- p_T neutrinos, resulting in large E_T^{miss} and m_T tails. In MC, the second lepton veto removes 45% of the dilepton $t\bar{t}$ and 10% of the single-lepton $t\bar{t}$ in the signal region. The veto performance is validated in the data in several control regions both enhanced and depleted in dilepton $t\bar{t}$, and in all cases the veto efficiencies in MC and data agree within 10%.

The next largest backgrounds come from single-lepton sources, including both W +jets and $t\bar{t}$ with one leptonic W decay. Both the normalization and the shape of the m_T distribution for this combined background are extracted from the data. First, the yield of the single lepton background estimated from simulation is normalized in the control region $60 \text{ GeV} < m_T < 90 \text{ GeV}$ to the data. Next, the shape of the m_T distribution in MC is compared with data in various control regions, where events satisfy the signal event selection but have fewer than four jets. Further, events with identified b -jets, based on lifetime b -tagging [32], are rejected in order to reduce the dilepton $t\bar{t}$ background, such that the samples are dominated by W +jets events; the corresponding loss of single-lepton $t\bar{t}$ from this b -jet veto is accounted for in the systematic uncertainties. Good agreement is observed between data and MC and based on this agreement an uncertainty of 15% is assigned on this background.

In general, QCD multi-jet events do not produce large E_T^{miss} and therefore fail the kinematic requirements for the signal region. Although the QCD multi-jet background is expected to be small, it is difficult to model with simulation. Therefore, data-driven techniques similar to those described in [32] are used to estimate this background. In both lepton channels the contribution to the signal region is consistent with zero.

Other electroweak processes, single top, diboson production (WW , WZ , and ZZ), and Z +jets are estimated using MC simulation, normalized to the theoretical cross section and total integrated luminosity. They have small production cross sections compared to $t\bar{t}$ and W +jets, and are further suppressed by the multiple-jet, E_T^{miss} and m_T selection criteria.

7. Background Estimate for Resonance Search

The following data-driven relative scale factors are applied to the simulated W +light parton multiplicity samples: 0-parton exclusive sample: 0.978 ± 0.004 ; 1-parton exclusive sample: 1.107 ± 0.015 ; 2-parton exclusive sample: 1.147 ± 0.047 ; 3-parton exclusive sample: 0.86 ± 0.16 ; 4-parton exclusive sample: 1.63 ± 0.44 ; 5-parton inclusive sample: 0.95 ± 0.58 . These are determined by fitting the observed jet multiplicity distribution in a W +jets-dominated data sample selected by: exactly one lepton with $p_T > 20 \text{ GeV}$, veto on the presence of any other lepton with $p_T > 10 \text{ GeV}$, $30 < E_T^{\text{miss}} < 80 \text{ GeV}$, $40 < M_T < 80 \text{ GeV}$, and rejection of events in which at least one of the four hardest jets is b -tagged. The latter cut ensures that the sample is orthogonal to the signal selection. The sample is expected to contain over 95% W +jets events, and remaining contributions from other Standard Model processes are subtracted using MC predictions prior to the fit. Note that the resulting scale factors are heavily anticorrelated, which is taken into account in the evaluation of systematic uncertainties. The uncertainties in the scale factors arise from the limited size of the data sample. This background's normalization uncertainty in the signal sample is 35%, driven by the uncertainty in the relative event tagging probabilities between events with two and four or more jets.

The QCD multi-jet background is estimated in the same way as described in Section 6. The $t\bar{t}$ and the other electroweak backgrounds are estimated using MC simulation, normalized to the theoretical cross section and total integrated luminosity.

8. Top Partner Search

Due to the small size of the data sample, and in order to preserve as much model-independence as possible, a simple cut-and-count analysis is carried out in the high tails of the W transverse mass and E_T^{miss} distributions. Figure 1 shows that the W transverse mass and E_T^{miss} tails are well modeled by SM contributions in two different control samples.

8.1. Systematic Uncertainties

The dilepton veto carries an uncertainty of 15%, determined in control regions in data described in Section 6. The single lepton shape correction, $S(m_T)$, was determined to be consistent with unity, but carries an uncertainty

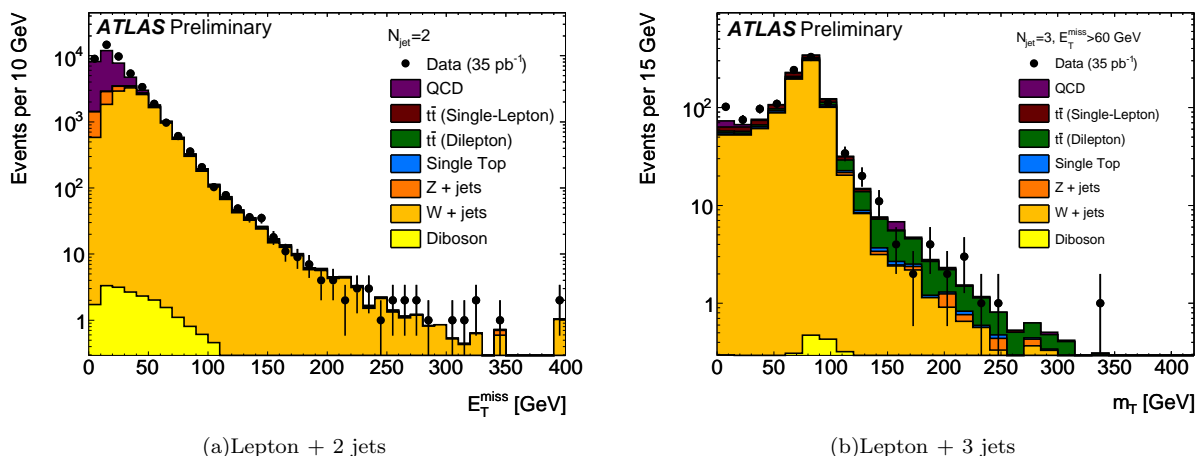


Figure 1: E_T^{miss} and m_T distributions in data and stacked simulation in two control samples of the top partner search, 2-jet events (a) and 3-jet events (b). $E_T^{\text{miss}} > 60$ GeV is required in (b).

of 15% from the spread in control regions. The single lepton normalization is taken from the W mass range (60-90 GeV) just outside the signal region. This normalization has an uncertainty of 10%, which is mostly the statistical uncertainty, but also includes the effect of varying the mass range used. The jet energy scale and resolution have some uncertainty [34], which is propagated through the analysis by correcting the jet multiplicity, m_T , and E_T^{miss} . The per-jet uncertainty ranges from more than 10% at low p_T to roughly 5% at high p_T . The Monte Carlo is adjusted for measured differences in lepton ID and trigger efficiencies, and these corrections each contribute some uncertainty, typically 4-5% per lepton. The integrated luminosity has a relative uncertainty of 3.4%.

8.2. Results

Comparing with the data, good agreement with the combined background prediction is observed: 17.2 background events are expected, and 17 events are observed. Figure 2 shows some distributions in the signal region. No evidence of an excess or of a mis-modeled background is observed. Given a theoretical cross section of 12 pb, an additional 12.4 ± 3.1 signal events are expected from the 275 GeV T (50 GeV A_0) mass point. Similarly, the 300 GeV T (10 GeV A_0) model would predict 11.7 ± 3.0 extra events from a cross section of 7.3 pb [37]. The event yield distribution is studied from pseudo-experiments, assuming Gaussian systematics and including correlations in signal and background systematics (*e.g.*, luminosity, theoretical cross sections), for both the signal and background-only hypotheses, and it is determined that both of these models can be excluded with confidence greater than 95%. The samples with $m(T)$ ($m(A_0)$) of 250 (10) GeV and 275 (10) GeV are excluded as well. Implicitly, all other mass points with a lighter A_0 are also excluded.

9. $t\bar{t}$ Resonance Search

9.1. Mass Reconstruction

To reconstruct the $t\bar{t}$ mass, the neutrino's longitudinal momentum (p_z) is determined by imposing the W -boson mass constraint. If the discriminant of the quadratic equation is negative, the missing transverse energy is adjusted to get a null discriminant [38]. If there are two solutions, the smallest p_z solution is chosen. The dominant source of long, non-Gaussian tails in the mass resolution is the use of a jet from initial- or final-state radiation in the place of one of the jets directly related to a top quark decay product. To reduce this contribution, the dR_{min} algorithm [13] considers the four leading jets with $p_T > 20$ GeV and $|\eta| < 2.5$, and excludes a jet if its angular distance to the lepton or closest jet satisfies $\Delta R_{min} > 2.5 - 0.015 \times m_j$, where m_j is the jet's mass. (If more than one jet satisfies this condition, the jet with the largest dR_{min} is excluded.) If a jet was discarded and more than three jets remain, the procedure is iterated. Then $m_{t\bar{t}}$ is reconstructed from the lepton, E_T^{miss} and the leading four jets, or three jets if only three remain. The ΔR_{min} cut removes jets

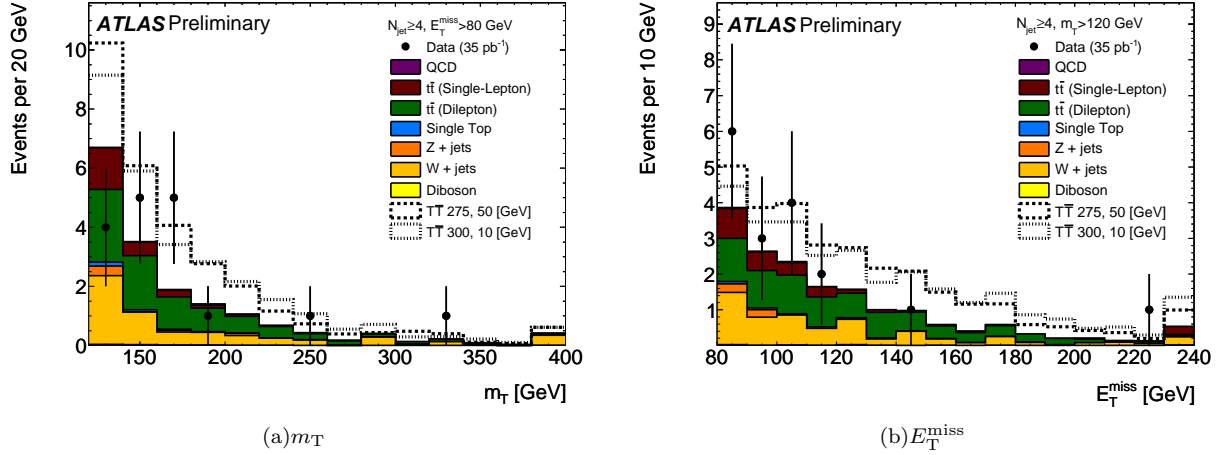


Figure 2: m_T and E_T^{miss} in the signal region of the top partner search. The dotted and dashed lines show the expected distributions for two of the excluded signal mass points, where the numbers in the legends correspond to $m(T)$ and $m(A_0)$.

that are “far” from the rest of the activity in the event. Furthermore, by only requiring three jets in the mass reconstruction, the method allows one of the jets from top quark decay to be outside the detector acceptance, or merged with another jet. The reconstructed invariant masses and corresponding resolutions obtained with the $dRmin$ algorithm are shown for three different simulated Z' boson masses in Fig. 3.

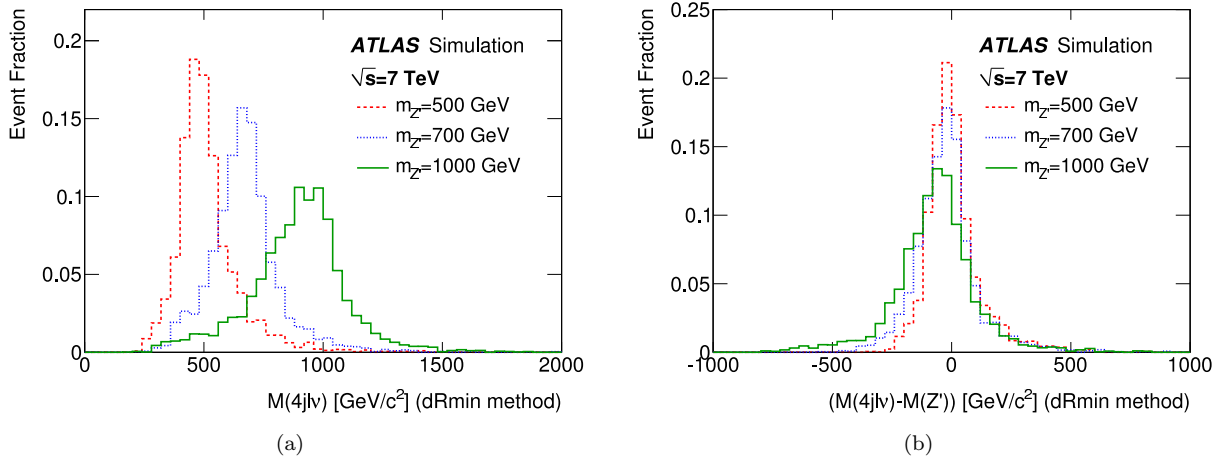


Figure 3: Reconstructed $t\bar{t}$ pair invariant mass (a) and its resolution (b) for three Z' boson masses: $m_{Z'} = 500$ GeV, $m_{Z'} = 700$ GeV and $m_{Z'} = 1000$ GeV for the $dRmin$ algorithms.

9.2. Systematic Uncertainties

Systematic uncertainties that only affect the normalization of the different backgrounds come from the uncertainty on the integrated luminosity (4.5%), background normalizations ($t\bar{t}$: $+7.0\%$ [39], single top: 10%, W +jets: 35%, diboson: 5%, QCD multi-jet(e): 30%, QCD multi-jet(μ): 50%), and lepton trigger and reconstruction efficiencies ($\leq 1.5\%$). The dominant shape uncertainties arise from the b -tagging efficiency (11% variation in the event yields), jet energy scale including pileup effects (9%) [34], and modelling of initial and final state radiation (7%). The first two have been determined from data by comparing results from different methods and/or data samples, while the latter has been estimated from MC simulations in which the relevant parameters were varied. Other uncertainties arising from MC modelling as well as lepton identification and momentum measurements have a substantially smaller impact.

9.3. Results

The results of this search are obtained by comparing the top quark pair invariant mass ($m_{t\bar{t}}$) distribution with background-only and signal-plus-background hypotheses. In practice, the search is done in two steps: in a first step the data is compared to the Standard Model prediction, i.e. the null hypothesis, using the BUMPHUNTER [40] algorithm. Since no excess is found, in a second step a limit is set using a Bayesian approach [41] on the maximum allowed cross-section times branching ratio for new physics as a function of $m_{t\bar{t}}$. In this limit-setting step, 40 GeV-wide bins are used, a value close to the mass resolution and limiting bin-by-bin statistical fluctuations. A single bin contains all events with $m_{t\bar{t}} > 2.96$ TeV.

The observed limits on narrow and wide resonances using the $dRmin$ mass reconstruction method are shown in Fig. 4 together with the predicted cross-section times branching ratio for the models considered and the expected sensitivity of the analysis. The observed (expected) limit on $\sigma \times BR(Z' \rightarrow t\bar{t})$ ranges from 38 (20) pb at $m_{Z'} = 500$ GeV to 3.2 (2.2) pb at $m_{Z'} = 1300$ GeV. While narrow resonances with production cross-sections predicted by the leptophobic topcolour model cannot be excluded, the analysis is already able to probe the few picobarn range for masses close to 1 TeV. The observed (expected) limit on $\sigma \times BR(g_{KK} \rightarrow t\bar{t})$ ranges from 32 (24) pb at $m_{g_{KK}} = 500$ GeV to 6.6 (2.9) pb at $m_{g_{KK}} = 1300$ GeV, which excludes g_{KK} resonances with mass below 650 GeV at 95% C.L.

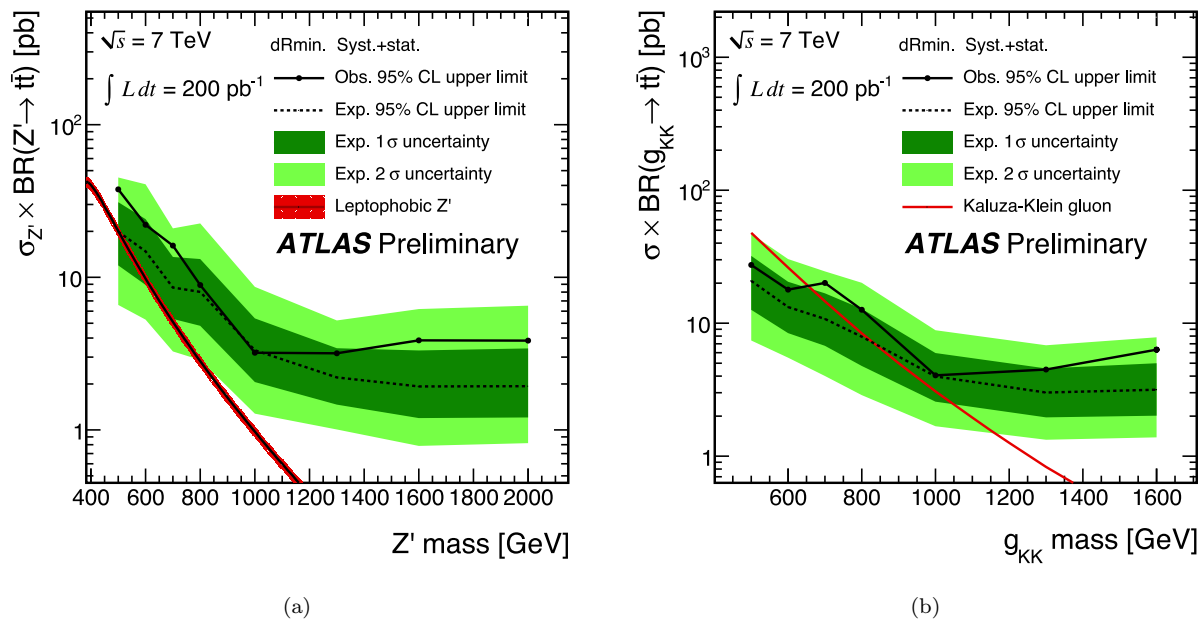


Figure 4: Expected (dashed line) and observed (black points connected by a line) upper limits on $\sigma \times BR(Z' \rightarrow t\bar{t})$ (a) and $\sigma \times BR(g_{KK} \rightarrow t\bar{t})$ (b) using the $dRmin$ algorithm. The dark and light green bands show the range in which the limit is expected to lie in 68% and 95% of experiments, respectively, and the red lines correspond to the predicted cross-section times branching ratio in the leptophobic topcolour and RS models. The error bars on the topcolour cross-section curve represent the effect of the PDF uncertainty on the prediction.

10. Summary and Conclusion

Two searches for new phenomena involving top quarks are presented: a search for a top partner in $t\bar{t}$ events with large missing transverse momentum, and a search for $t\bar{t}$ resonances in 35 pb^{-1} and 200 pb^{-1} of data, respectively. No evidence for a signal is observed and 95% C.L. limits are set on benchmark models. Both analyses are currently being updated with more luminosity [42].

References

- 1 ATLAS Collaboration, J. Instrum. **3**, S08003 (2008).
- 2 ATLAS Collaboration, ATLAS-CONF-2011-036 (2011).
- 3 T. Han, R. Mahbubani, D. G. E. Walker and L. T. E. Wang, J. High Energy Phys. **0905**, 117 (2009).
- 4 J. Alwall, J. L. Feng, J. Kumar and S. Su, Phys. Rev. D **81**, 114027 (2010);
- 5 N. Arkani-Hamed, A. G. Cohen and H. Georgi, Phys. Lett. B **513**, 232 (2001); H. C. Cheng and I. Low, J. High Energy Phys. **0309**, 051 (2003); H. C. Cheng and I. Low, J. High Energy Phys. **0408**, 061 (2004); H. C. Cheng, I. Low and L. T. Wang, Phys. Rev. D **74**, 055001 (2006).
- 6 T. Appelquist, H. C. Cheng and B. A. Dobrescu, Phys. Rev. D **64**, 035002 (2001).
- 7 P. Fileviez Perez and M. B. Wise, Phys. Rev. D **82**, 011901 (2010).
- 8 V. M. Abazov *et al.*, D0 Collaboration, Phys. Rev. Lett. **101**, 241802 (2008).
- 9 ATLAS Collaboration, ATLAS-CONF-2011-087 (2011).
- 10 T. Aaltonen *et al.*, CDF Collaboration, Phys. Rev. Lett. **100**, 231801 (2008).
- 11 T. Aaltonen *et al.*, CDF Collaboration, Phys. Rev. D **77**, 051102 (2008); T. Aaltonen *et al.*, CDF Collaboration, Phys. Lett. B **691**, 183 (2010).
- 12 V. M. Abazov *et al.*, D0 Collaboration, Phys. Lett. B **668**, 98 (2008).
- 13 ATLAS Collaboration, ATLAS-CONF-2011-070 (2011).
- 14 CMS Collaboration, CMS-PAS-TOP-10-007 (2010).
- 15 C. T. Hill, and S. J. Parke, Phys. Rev. D **49**, 4454 (1994).
- 16 R. M. Harris, C. T. Hill, and S. J. Parke, arXiv:hep-ph/9911288 (1999).
- 17 C. T. Hill, Phys. Lett. B **345**, 483 (1995).
- 18 B. Lillie, L. Randall, and L.-T. Wang, JHEP **09**, 074 (2007).
- 19 A. Djouadi, G. Moreau, and R. K. Singh, Nucl. Phys. B **797**, 1 (2008); B. C. Allanach, F. Mahmoudi, J. P. Skittrall, and K. Sridhar, arXiv:0910.1350 [hep-ph] (2009).
- 20 ATLAS Collaboration, ATLAS-PHYS-PUB-2010-008 (2010).
- 21 J. Alwall, P. Demin, S. de Visscher, R. Frederix, M. Herquet, et al., JHEP **0709**, 028 (2007), arXiv:0706.2334 [hep-ph] (2007).
- 22 ATLAS Collaboration, Eur. Phys. J. C **70**, 823 (2010).
- 23 S. Agostinelli et al., Nucl. Instrum. Methods Phys. Res., Sect. A **506**, 250 (2003).
- 24 S. Frixione and B. R. Webber, J. High Energy Phys. **0206**, 029 (2002).
- 25 M. L. Mangano et al., J. High Energy Phys. **0307**, 001 (2003).
- 26 G. Corcella et al., J. High Energy Phys. **0101**, 010 (2001).
- 27 J. M. Butterworth, J. R. Forshaw, and M. H. Seymour, Z. Phys. C **72**, 637 (1996).
- 28 K. Melnikov and F. Petriello, Phys. Rev. D **74**, 114017 (2006).
- 29 J. M. Campbell, R. K. Ellis, and D. L. Rainwater, Phys. Rev. D **68**, 094021 (2003).
- 30 T. Sjöstrand, S. Mrenna, and P. Skands, J. High Energy Phys. **0605**, 026 (2006).
- 31 M. Aliev, H. Lacker, U. Langenfeld, S. Moch, P. Uwer, M. Wiedermann, Comput.Phys.Comm. **182**, 1034 (2011).
- 32 ATLAS Collaboration, Eur. Phys. J. C **71**, 1577 (2011).
- 33 M. Cacciari, G. P. Salam, and G. Soyez, J. High Energy Phys. **0804**, 063 (2008).
- 34 ATLAS Collaboration, ATLAS-CONF-2011-007 and ATLAS-CONF-2011-032 (2011).
- 35 ATLAS Collaboration, J. High Energy Phys. **1012**, 060 (2010).
- 36 ATLAS Collaboration, ATLAS-CONF-2010-099 (2010).
- 37 E. Berger and Q.-H. Cao, arXiv:09093555 [hep-ph] (2009).
- 38 T. Chwalek, Ph.D. Thesis, IEKP-KA/2010-5, KIT Karlsruhe (2010).
- 39 S. Moch and P. Uwer, Phys. Rev. D **78**, 034003 (2008).
- 40 G. Choudalakis, arXiv:1101.0390 [physics.data-an] (2011).
- 41 I. Bertram *et al.*, D0 Collaboration, FERMILAB-TM-2104 (2000).
- 42 ATLAS Collaboration, CERN-PH-EP-2011-149, submitted to Phys. Rev. Lett., arXiv:1109.4725v1 [hep-ex] (2011).